Journal Name

ARTICLE

Engineering high-performance and air-stable PBTZT-stat-BDTT-8:$PC_{61}BM$/$PC_{71}BM$ organic solar cells

Received 00th January 20xx,
Accepted 00th January 20xx

DOI: 10.1039/x0xx00000x

www.rsc.org/

Il Jeon,[a] Ryohei Sakai,[b] Seungju Seo,[a] Graham E. Morse,[c] Hiroshi Ueno,[d] Takafumi Nakagawa,[a] Yang Qian,[a] Shigeo Maruyama,[a,e] Yutaka Matsuo[a,f]*

High-performance air-stable PBTZT-stat-BDTT-8 organic solar cells were fabricated using mixed C_{60}/C_{70} fullerene acceptors. Normal-architecture devices using PBTZT-stat-BDTT-8 with $PC_{71}BM$ produced a power conversion efficiency (PCE) of 9.38%. Inverted-architecture, which possess higher stability, was fabricated using a more economical $PC_{61}BM$ and $PC_{71}BM$ mixture with solution-processed PEDOT:PSS on top, and produced a PCE of 8.15%. Exploiting the viscous nature of PBTZT-stat-BDTT-8, the slow evaporation effect was utilised to achieve an even higher efficiency of 8.73%. The stability test was conducted under operating condition and our devices showed remarkably higher stability compared with PTB7-based devices.

Organic solar cells (OSCs) have received much attention as the next-generation of clean and efficient light-harvesting devices in recent years.[1–8] Their highest reported power conversion efficiency (PCE) now exceeds 10% in a non-tandem device.[9,10] As OSC technology matures, there are more important aspects to consider than efficiency, namely scalability,[11] stability,[12] and fabrication cost.[13] Currently, low band-gap polymer donors, such as thieno[3,4-b]thiophene/benzodithiophene (PTB7) family polymers, are top performers in the field of OSCs.[14–16] However, PTB7 family polymers are not good candidates from an industrial perspective because they require chlorinated solvents and a toxic iodinated hydrocarbon additive, 1,8-diiodooctane (DIO).[10,17–19] Also, the low mobility of PTB7 limits the film thickness to be less than 120 nm.[20] As a result, these issues prevent scalable manufacturing processes, such as roll-to-roll processing, spray coating, and slot die coating.[21,22] Furthermore, the intrinsic instability of PTB7 to air, water, and light is a major obstacle.[23,24] Towards this end, it is imperative to use the inverted architecture, which achieves stability by avoiding the use of low-work-function metals and direct contact between poly(3,4-ethylenedioxythiophene) polystyrene sulfonate (PEDOT:PSS) and indium tin oxide (ITO).[25,26] However, the vulnerability of PTB7 to water means that low-cost solution-processed PEDOT:PSS cannot be used, and the choice of the hole-transporting layer (HTL) is limited to materials such as MoO_3 that are thermally deposited in vacuum.[24,27]

PBTZT-stat-BDTT-8 is a low band-gap polymer with a band gap of 1.7 eV and consists of substituted benzodithiophene, thiophene, and benzothiadiazole.[28–32] PBTZT-stat-BDTT-8 is compatible with non-chlorinated solvents, *o*-xylene, and tetralin, without the use of DIO as an additive.[29,33–35] Excellent stability in air and high carrier mobility are the two main advantages of this copolymer.[35,38] To date, the highest PCEs reported for PBTZT-stat-BDTT-8-based OSCs are 8.5% and 7.2% for standard and inverted architectures, respectively.[35,36] The difference in PCE between the standard and inverted structures is rather large for PBTZT-stat-BDTT-8-based devices. Different molecular orientations of the copolymer are assumed to be the reason behind this.[37]

In this work, high-performance low-cost OSCs in the standard (Fig. 1a) and inverted architectures (Fig. 1b) were demonstrated using PBTZT-stat-BDTT-8 and a mixture of phenyl-C_{61}-butyric acid methyl ester ($PC_{61}BM$) and phenyl-C_{71}-butyric acid methyl ester ($PC_{71}BM$) (Fig. 1c). We exploited the slow evaporation effect of PBTZT-stat-BDTT-8 to improve the efficiency of the inverted architecture with PEDOT:PSS. Standard-type OSCs with a combination of PBTZT-stat-BDTT-8 and $PC_{71}BM$ gave a PCE of 9.38% (an average of 9.20%) while using mix-PCBM[38] gave a PCE of 8.96%. A PCE of 8.15% was obtained from inverted OSCs with mix-PCBM and an even higher PCE of 8.73% was obtained by employing slow evaporation.[39] The mix-PCBM-based inverted devices were fabricated using PEDOT:PSS as the HTL and exhibited substantially higher stability compared with PTB7-based devices.

[a] *Department of Mechanical Engineering, School of Engineering, The University of Tokyo, 7-3-1 Hongo, Bunkyo-ku, Tokyo 113-8656, Japan. E-mail: matsuo@photon.t. u-tokyo.ac.jp*
[b] *Fujipream Corporation, 38-1 Shikisai, Hyogo 671-2216, Himeji, Japan*
[c] *Merck Chemicals Ltd., Chilworth Technical Centre, University Parkway, SO16 7QD Southampton, UK*
[d] *School of Chemistry, Northeast Normal University, Changchun, Jilin 130024, China*
[e] *National Institute of Advanced Industrial Science and Technology (AIST), 1-2-1 Namiki, Tsukuba, Ibaraki 305-8564, Japan*
[f] *Hefei National Laboratory for Physical Sciences at the Microscale, University of Science and Technology of China, Hefei, Anhui 230026, China*
Electronic Supplementary Information (ESI) available: [details of any supplementary information available should be included here]. See DOI: 10.1039/x0xx00000x

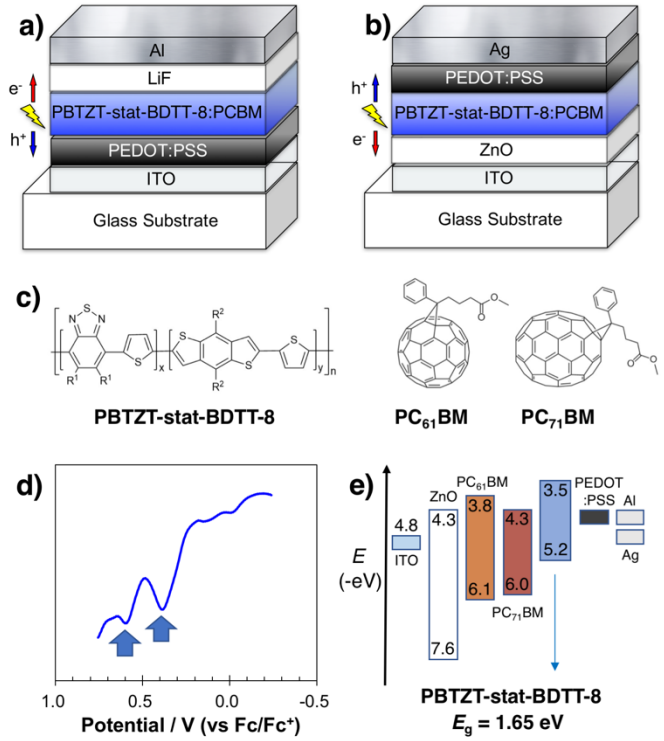

Fig. 1 Schematics of PBTZT-stat-BDTT-8-based solar cells (a) in a normal architecture and (b) in an inverted architecture. (c) Molecular structures of PBTZT-stat-BDTT-8, $PC_{61}BM$, and $PC_{71}BM$. Electrochemical property and comparison with electron-accepting materials. (d) Differential pulse voltammetry in *o*-DCB /dichloromethane (1/1) containing $(n\text{-Bu})_4NPF_6$ supporting electrolyte (0.1 M) at room temperature. The first oxidation potential was 0.39 V vs Fc/Fc^+. (e) Energy levels of the device layers used in this work, including the PBTZT-stat-BDTT-8, E_g of which was determined from the offset of the absorption spectrum.[35]

Results and discussion

Material characterisation and device optimisation

As the first step of the investigation, we carried out cyclic voltammetry (CV) and differential pulse voltammetry (DPV) (Fig. S1). DPV measurement with *ortho*-dichlorobenzene (*o*-DCB)/CH_2CH_2 1:1 mixture gave a clear potential, which was used in a combination with the absorption spectrum[35] to determine the energy gap (E_g) to be 1.65 eV (Fig. 1d). Using this, energy diagrams of the devices have been drawn (Fig. 1e). Based on the energy diagram, standard-type OSCs were fabricated and optimised with respect to the electrode (Fig. S2), concentration of the spin-coating solution (Fig. S3), donor-to-acceptor ratio (Fig. S4), spinning speed (Fig S5), spin-coating time (Fig. S6), and thermal annealing conditions (Fig. S7). Unlike in previous reports,[35,36] an Al electrode with a 1:3 donor-to-acceptor ratio gave the best performance for our devices (Fig. S8). In addition, due to the highly viscous nature of PBTZT-stat-BDTT-8 solution, spin-coating while the solution was hot without using a filter resulted in higher performance. Solvent compatibility tests revealed that the PBTZT-stat-BDTT-8-based devices showed high performance for all tested solvents types and additives (Fig. S9). Having confirmed this, we used *o*-DCB without additives for all experiments. As the next step, we used three different types of PCBM electron acceptors. Fig. 2a shows that the PBTZT-stat-BDTT-8 and $PC_{71}BM$ combination-based devices gave a PCE of 9.38%. To the best of our knowledge, this is a record-high efficiency, but the $PC_{71}BM$ acceptor is known to be more costly.[40,41] Therefore, less costly counterparts $PC_{61}BM$ and mix-PCBM were tested. The $PC_{61}BM$-based devices gave a PCE of 8.84% and the mix-PCBM-based devices gave a PCE of 8.96%. The solar cells using mix-PCBM gave a slightly higher PCE compared with the $PC_{61}BM$-based devices. This subtle difference was due to the higher open-circuit voltage (V_{OC}) of the mix-PCBM device, which is expected for the standard architecture according to our previous report.[38]

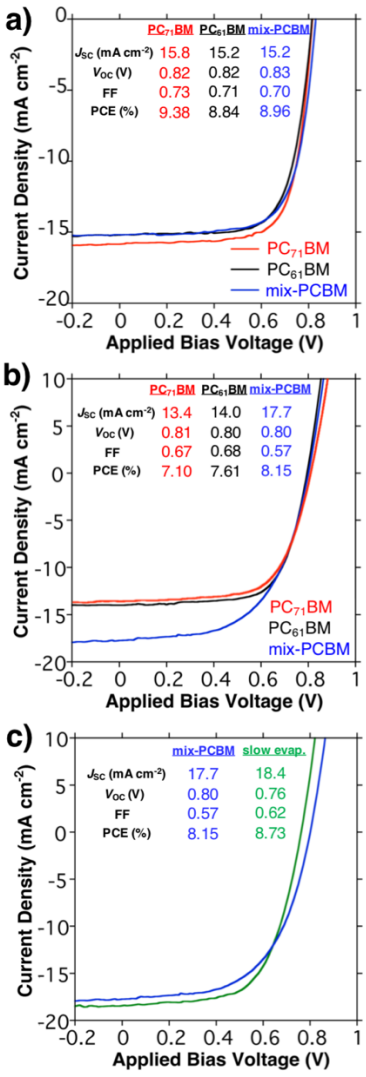

Fig. 2 (a) *J-V* curves of normal type PBTZT-stat-BDTT-8 solar cells with $PC_{71}BM$, $PC_{61}BM$, and mix-PCBM as the electron acceptor. *J-V* curves of inverted type PBTZT-stat-BDTT-8 solar cells with (b) $PC_{71}BM$, $PC_{61}BM$, and mix-PCBM as the electron acceptor; and (c) the effect of the slow evaporation on the devices with mix-PCBM as the electron acceptor.

Inverted architecture via slow evaporation

For the perspective of power generation, the stability of OSCs can be considered the most important factor. In this

regard, the standard architecture is likely not the best choice, because it utilises metal electrodes with a high work function and acidic PEDOT:PSS is in direct contact with the ITO electrode.[25,28] Therefore, we tested inverted OSCs using aqueous solution-processed PEDOT:PSS as the HTL on the active layer (Fig. 1b). Fig. 2b shows that high PCE values were obtained unlike PTB7-based devices (Table 1). We attribute this to the intrinsic high stability of PBTZT-stat-BDTT-8 against water. The photovoltaic data in Fig. 2b also show that the $PC_{71}BM$-based devices gave a PCE of 7.10%, which is lower than that of the $PC_{61}BM$-based devices (7.61%). The mixed PCBM-based devices, to our surprise, displayed the highest PCE among the inverted devices with a PCE of 8.15%. This higher PCE was due to its higher short-circuit current density (J_{SC}), which arose from the greater interpenetrating area in the amorphous phase of mix-PCBM.[38,42] On the other hand, the fill factor (FF) of the mix-PCBM-based device was decreased because of the inherently lower electron mobility of mix-PCBM compared with $PC_{61}BM$ or $PC_{71}BM$.[43,44] Nevertheless, PCEs were lower for all of the inverted devices compared with the standard-type devices. We suspect that different molecular orientations of the copolymer[37] were the reason for this phenomenon, given that some polymers exhibit similar behaviour.[45] To address this, the slow evaporation effect was employed to improve the PCE of the mix-PCBM-based inverted OSCs.[39] PTB7 has low mobility, which means that the film has to be thin. So a high-spin-speed coating results in a dry film. However, PBTZT-stat-BDTT-8 has high mobility which allows fabrication of a thick active layer, which is wet after a low-speed spin-coating. Accordingly, by drying the film slowly, vertical separation can be induced in which fullerene acceptors migrate to the bottom and the polymer donors migrate to the top within the blend (Fig. S10).[46,47] As shown in Fig. 2c, the PCE increased from 8.15% to 8.73% as a result of slow evaporation. The increase in FF and J_{SC} was due to favourable vertical separation.

Stability investigation of polymer

Having obtained high PCE by slow evaporation, stability of the device was investigated. Vulnerability of the polymer donor against oxygen and moisture is crucial to overall device performance and processing technique. X-ray photoelectron spectroscopy (XPS) reveals information as to degradation of the polymers over time. Fig. 3a to 3f show XPS data of PTB7 and PBTZT-stat-BDTT-8 thin films in ambience (40 °C, relative humidity 40%) before and after one week. It is evident that PTB7 was oxidised substantially after one week. The $S2p_{3/2}$ and $2p_{1/2}$ doublet with the $2p_{3/2}$ component at 164 eV is typical of S from C-S bonds in the polymer donors (Fig. 3a and d).[48] After one week, the doublets become less defined which is due to the sulphoxide peak (S=O) in the middle of the doublet by hydration.[49,50] The appearance of an S peak associated with a sulphone group, $-SO_3^-$ at 168 eV confirms degradation in PTB7, which is not observed in the XPS spectrum of PBTZT-stat-BDTT-8 (Fig. 3d).[48,51] The C1s peak shows a symmetric hydrocarbon-like main component at 284 eV due to C–C bonding in the side chains and aromatic rings (Fig. 3b and e). Two weak components are from C-S at 287 eV and -O–C=O at 289 eV, which intensified after oxidation, revealing stronger oxidation in PTB7 compared with PBTZT-stat-BDTT-8.[48,52] The O1s peak in Fig 3c is broadened after one week, which indicates generation of C=O at *ca.* 531 eV and C–O at ca. 533 eV.[48,52] In the case of PBTZT-stat-BDTT-8, this only marginal generation of C–O was observed (Fig. 3f). Looking at the intensity of the O peaks, it is clear that PBTZT-stat-BDTT-8 does not undergo oxidation as strong as PTB7. Overall, the peaks of PBTZT-stat-BDTT-8 shifted to higher energy, which is a good indication of stronger oxidation and degradation.

Stability investigation of bulk-heterojunction

The bulk-heterojunction blend of polymer donor with mix-PCBM is reported to be more rigid than that with $PC_{61}BM$, because the heterogeneous character of the $PC_{61}BM$ and $PC_{71}BM$ mixture introduces crystal defects that prevent the domains from becoming large.[38,53] The same was true for the PBTZT-stat-BDTT-8:mix-PCBM blend as observed in the atomic force microscopy (AFM) surface analyses (Fig. S11). After annealing at 200 °C for 2 hours, the arithmetic mean surface roughness (R_a) of the PBTZT-stat-BDTT-8:mix-PCBM film had less change in its domains compared with $PC_{61}BM$. Space-charge-limited current (SCLC) mobility data also corroborate excellent stability of PBTZT-stat-BDTT-8:mix-PCBM blend. Table 1 shows that the hole mobility of PBTZT-stat-BDTT-8:mix-PCBM is higher than those of $PC_{61}BM$ and $PC_{71}BM$ (Fig. S12). This is due to low crystallinity of mix-PCBM in the blend. Despite low electron mobility compared to of $PC_{61}BM$ and $PC_{71}BM$

Table 1. Photovoltaic parameters of various devices recorded under 1 sun illumination (100 mW cm^{-2}, AM 1.5 G).

Type	Active Layer	HTL	V_{OC} (V)	J_{SC} (mA cm^{-2})	FF	PCE (%)
Normal	PBTZT-stat-BDTT-8:$PC_{71}BM$	LiF	0.82	15.8	0.73	9.38
	PBTZT-stat-BDTT-8:$PC_{61}BM$		0.82	15.2	0.71	8.84
	PBTZT-stat-BDTT-8:mix-PCBM		0.83	15.2	0.70	8.96
Inverted	PBTZT-stat-BDTT-8:$PC_{71}BM$	PEDOT:PSS	0.81	13.4	0.67	7.10
	PBTZT-stat-BDTT-8:$PC_{61}BM$		0.80	14.0	0.68	7.61
	PBTZT-stat-BDTT-8:mix-PCBM		0.80	17.7	0.57	8.15
	↳slow evaporation		0.76	18.4	0.62	8.73
	PBT7:$PC_{71}BM$		0.64	9.56	0.41	2.70
	PBT7:$PC_{71}BM$	MoO_3	0.78	15.8	0.63	7.81

counterparts (Fig. S13), PBTZT-stat-BDTT-8:mix-PCBM retained its mobility after ageing (Fig. S14). Since it is both the hole and electron mobilities that we have to consider, we can conclude that the stability of mix-PCBM-used bulk heterojunction is high. The stability of the PBTZT-stat-BDTT-8:mix-PCBM blend in the inverted solar cells was tested in air under constant illumination without encapsulation. For reference, we included data on two PTB7:$PC_{71}BM$ devices, one with a MoO_3 HTL and one with a PEDOT:PSS HTL. As shown in Fig. 3g, the PBTZT-stat-BDTT-8:mix-PCBM devices were significantly more stable than the PTB7:$PC_{71}BM$ devices (Fig. S15). PTB7-based devices with aqueous PEDOT:PSS in contact with the active later displayed a rapid drop in PCE, indicating that the stability of PBTZT-stat-BDTT-8 to water enables the use of solution-processed PEDOT:PSS.

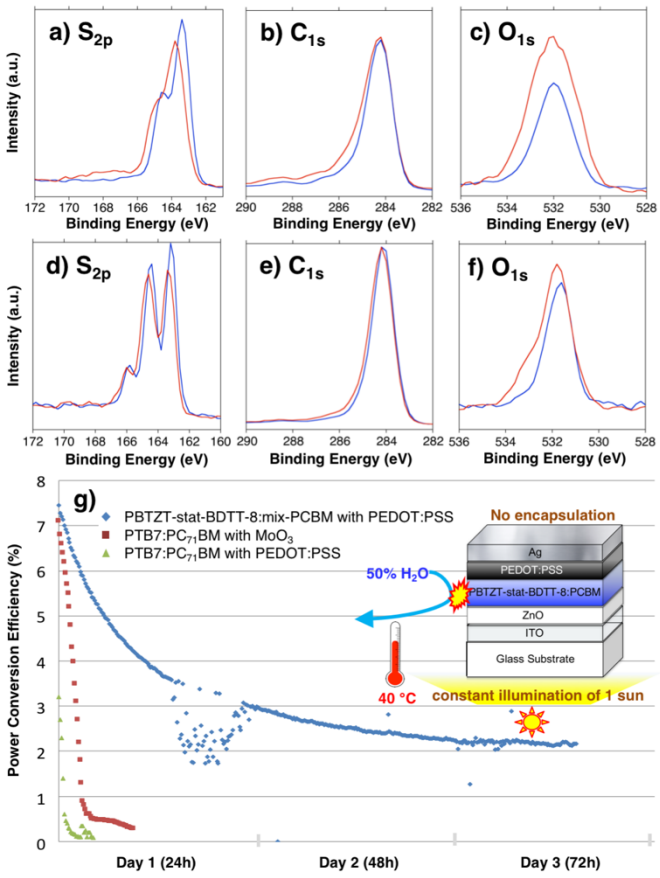

Fig. 3 XPS spectra of PTB7 (a) S2p, (b) C1s, (c) O1s, and PBTZT-stat-BDTT-8 (d) S2p, (e) C1s, (f) O1s, before (blue line) and after one week in ambience (red line). (g) Stability of unencapsulated OSCs under constant illumination of 1 sun in humid air (40 °C, 50% relative humidity) for PBTZT-stat-BDTT-8:mix-PCBM (in blue diamond), PTB7:$PC_{71}BM$ with MoO_3 (in red square) or PEDOT:PSS (in green triangle).

Conclusions

In conclusion, both the standard and inverted architectures of PBTZT-stat-BDTT-8-based solar cells were fabricated using different PCBMs. Mixed-PCBM-based devices showed higher performance and stability compared with $PC_{61}BM$- or $PC_{71}BM$-based inverted OSCs. Exploiting the viscous nature of PBTZT-stat-BDTT-8 solution, the slow evaporation effect was employed and improved the efficiency to 8.73% through the use of aqueous solution-processable PEDOT:PSS. The inverted devices displayed a remarkably high stability compared with the PTB7-based devices.

Experimental Section

Device fabrication

Patterned ITO substrates (15 x 15 mm) with a sheet resistance of 9 Ω sq^{-1} (Techno Print Co., Ltd.) were used. The substrates were sonicated sequentially in cleaning surfactant (Semi Clean, M-Lo), water, acetone and 2-isopropanol for 15 min each. The ITO substrates were exposed to UV/O_3 for 15 min. For the standard devices, a PEDOT:PSS dispersion in water (CleviosPVP, Heraeus Precious Metals GmbH & Co.) was spin-coated on ITO at 4500 rpm for 45 s. This was followed by the active layer deposition at 1000 rpm for 30 s for the best performance. LiF and Al were thermally deposited with thicknesses of 1 nm and 100 nm, respectively.

For the inverted devices, ZnO was fabricated by using the sol-gel method in which a 0.1 M solution of zinc acetate dihydrate [$Zn(CH_3COO)\cdot(2H_2O)$] (Wako, 99.0%) in ethanol (Wako, 99.5%) was stirred at 80 °C for 2–3 h. Next, ethanolamine stabilizer (28% in weight) was added and the solution was left stirring for a further 12-15 h at 60 °C. The solution was spin-coated on ITO at 3000 rpm for 30 s. After the deposition of the active layer, either 30-nm thick MoO_3 or modified PEDOT:PSS was deposited by thermal evaporation and spin-coating at 4000 rpm for 45 s, respectively. The modified PEDOT:PSS contains 0.5wt% polyoxyethylene(6) tridecyl ether (Sigma Aldrich Chemical Co., Inc.).

For the PBTZT-stat-BDTT-8 photoactive layer deposition, a mixture of [6,6]-phenyl C61-butyric acid methyl ester and [6,6]-phenyl C71-butyric acid methyl ester in 16:3 ratio (mix-PCBM) (Frontier Carbon Co., Nanom spectra E124) solution with a donor:acceptor ratio of 1:3 and concentration of 60 mg ml^{-1} in ortho-dichlorobenzene (anhydrous, 99%, Sigma Aldrich Chemical Co., Inc.) was prepared. The solution was left stirring for 2 h at 100 °C. The active solution was spin-coated onto target substrates at 1000 rpm for 30 s without a filtre and kept inside a Petri dish for 40 min for inducing the waiting effect. The devices were annealed at 100 °C for 10 min after the deposition of the top electrodes.

Characterisations

J-V characteristics were measured by using a software-controlled source meter (2400, Keithley) under dark conditions and 1 sun AM 1.5 G simulated sunlight irradiation (100 mW cm^{-2}) with a solar simulator (EMS-35AAA, Ushio Spax Inc.), which was calibrated by using a silicon diode (BS-520BK, Bunkoukeiki). UV-vis absorption spectra were measured with a spectrometer (V-670, JASCO) at room temperature (298 K) on a 1.5 x 1.5 cm glass substrate. Atomic force microscopy (AFM; Multi-mode, Bruker) topography images were recorded in tapping mode.

Silicon AFM probes, with a nominal frequency of 70 kHz. The structure of the electron-only devices was Al(100 nm)/active layer/LiF(0.6 nm)/Al(100 nm) and hole-only devices was ITO/PEDOT:PSS/active layer/MoO_3(10 nm)/Al(100 nm). The mobility was determined by fitting the dark current to a model of a single-carrier SCLC, which is described by the equation: $J = \frac{9}{8}\varepsilon_0\varepsilon_r\mu\frac{V^2}{L^3}$, where *J* is the current density, μ is the mobility, ε_0 is the permittivity of free space, ε_r is the relative permittivity of the material, *L* is the thickness of the active layer, and *V* is the effective voltage. The thickness of the BHJ layer was measured with a DEKTAK 6M stylus profilometer. A blended solution of PBTZT-stat-BDTT-8:mix-PCBM, $PC_{61}BM$ and $PC_{71}BM$ were spin-coated onto the Al/glass to form the active layer in electron-only devices, and onto the PEDOT:PSS in hole-only devices. The LiF/Al electrodes (LiF = 0.6 nm; Al = 100 nm) or MoO_3/Al were evaporated onto the active layer in the electron-only devices and hole-only devices, respectively. The experimental dark current density *J* of both PBTZT-stat-BDTT-8:mix-PCBM, $PC_{61}BM$ and $PC_{71}BM$ was measured under an applied voltage swept from –5 to 5 V.

Conflicts of interest

There are no conflicts to declare

Acknowledgements

We thank the Research and Education Consortium for Innovation of Advanced Integrated Science by Japan Science and Technology (JST). This work was supported by Japan Society for the Promotion of Science (JSPS) KAKENHI Grants JP15H05760, JP16H04187, JP17K19116, and JP17H06609.

Notes and references

1 K.-G. Lim, S. Ahn, Y.-H. Kim, Y. Qi and T.-W. Lee, *Energy Environ. Sci.*, 2016, **9**, 932–939.

2 G. Dennler, M. C. Scharber and C. J. Brabec, *Adv. Mater.*, 2009, **21**, 1323–1338.

3 G. Li, R. Zhu and Y. Yang, *Nat. Photonics*, 2012, **6**, 153–161.

4 H. Kim, J. Byun, S.-H. Bae, T. Ahmed, J.-X. Zhu, S.-J. Kwon, Y. Lee, S.-Y. Min, C. Wolf, H.-K. Seo, J.-H. Ahn and T.-W. Lee, *Adv. Energy Mater.* 2016, **6**, 1600172.

5 I. Jeon and Y. Matsuo, in Encyclopedia of Polymer Science and Technology, John Wiley & Sons, Inc., Hoboken, NJ, USA, 2017, pp. 1–21.

6 Z. Xiao, F. Liu, X. Geng, J. Zhang, S. Wang, Y. Xie, Z. Li, H. Yang, Y. Yuan and L. Ding, *Sci. Bull.*, 2017, **62**, 1331–1336.

7 M. An, F. Xie, X. Geng, J. Zhang, J. Jiang, Z. Lei, D. He, Z. Xiao and L. Ding, *Adv. Energy Mater.*, 2017, **7**, 1602509.

8 Z. Xiao, X. Geng, D. He, X. Jia and L. Ding, *Energy Environ. Sci.*, 2016, **9**, 2114–2121.

6 Y. Liu, J. Zhao, Z. Li, C. Mu, W. Ma, H. Hu, K. Jiang, H. Lin, H. Ade and H. Yan, *Nat. Commun.*, 2014, **5**, 5293.

7 Z. Xiao, X. Jia, and L. Ding, *Sci. Bull.*, 2017, **62**, 1562–1564.

8 S. Yoo, J. Lee, D. Han and H. Kim, in *Large Area and Flexible Electronics*, Wiley-VCH Verlag GmbH & Co. KGaA, Weinheim, Germany, 2015, pp. 439–468.

9 I. Jeon, R. Sakai, T. Nakagawa, H. Setoguchi and Y. Matsuo, *Org. Electron.*, 2016, **35**, 193–198.

10 T. T. Larsen-Olsen, R. R. Søndergaard, K. Norrman, M. Jørgensen and F. C. Krebs, *Energy Environ. Sci.*, 2012, **5**, 9467.

11 Z. He, C. Zhong, S. Su, M. Xu, H. Wu, Y. Cao, A. K. K. A. Kyaw, D. D. H. Wang, V. Gupta, J. Zhang, S. Chand, G. C. Bazan and A. J. Heeger, *Nat. Photonics*, 2013, **25**, 593–597.

12 Z. Xiao, X. Jia, D. Li, S. Wang, X. Geng, F. Liu, J. Chen, S. Yang, T. P. Russell and L. Ding, *Sci. Bull.*, 2017, **62**, 1494–1496.

13 L. Ye, X. Jiao, H. Zhang, S. Li, H. Yao, H. Ade and J. Hou, *Macromolecules*, 2015, **48**, 7156–7163.

14 C. Sprau, F. Buss, M. Wagner, D. Landerer, M. Koppitz, A. Schulz, D. Bahro, W. Schabel, P. Scharfer and A. Colsmann, *Energy Environ. Sci.*, 2015, **8**, 2744–2752.

15 M. V. Srinivasan, N. Tsuda, P.-K. Shin and S. Ochiai, *RSC Adv.*, 2015, **5**, 56262–56269.

16 Y. Liang, Z. Xu, J. Xia, S.-T. Tsai, Y. Wu, G. Li, C. Ray and L. Yu, *Adv. Mater.*, 2010, **22**, E135–E138.

17 B. Ebenhoch, S. A. J. Thomson, K. Genevičius, G. Juška and I. D. W. Samuel, *Org. Electron.*, 2015, **22**, 62–68.

18 Y. Zheng, T. Goh, P. Fan, W. Shi, J. Yu and A. D. Taylor, *ACS Appl. Mater. Interfaces*, 2016, **8**, 15724–15731.

19 H. Choi, S.-J. Ko, T. Kim, P.-O. Morin, B. Walker, B. H. Lee, M. Leclerc, J. Y. Kim and A. J. Heeger, *Adv. Mater.*, 2015, **27**, 3318–3324.

20 J. Razzell-Hollis, J. Wade, W. C. Tsoi, Y. Soon, J. Durrant and J.-S. Kim, *J. Mater. Chem. A*, 2014, **2**, 20189–20195.

21 D. Bartesaghi, G. Ye, R. C. Chiechi and L. J. A. Koster, *Adv. Energy Mater.*, 2016, **6**, 1502338.

22 Z. He, C. Zhong, S. Su, M. Xu, H. Wu and Y. Cao, *Nat. Photonics*, 2012, **6**, 593–597.

23 I. Jeon, J. W. Ryan, T. Nakazaki, K. S. Yeo, Y. Negishi and Y. Matsuo, *J. Mater. Chem. A*, 2014, **2**, 18754–18760.

24 J. You, C.-C. Chen, L. Dou, S. Murase, H.-S. Duan, S. A. Hawks, T. Xu, H. J. Son, L. Yu, G. Li and Y. Yang, *Adv. Mater.*, 2012, **24**, 5267–5272.

25 C. Menelaou, S. Tierney, N. Blouin, W. Mitchell, P. Tiwana, I. McKerracher, C. Jagadish, M. Carrasco and L. M. Herz, *J. Phys. Chem. C*, 2014, **118**, 17351–17361.

26 L. Lucera, F. Machui, P. Kubis, H. D. Schmidt, J. Adams, S. Strohm, T. Ahmad, K. Forberich, H.-J. Egelhaaf and C. J. Brabec, *Energy Environ. Sci.*, 2016, **9**, 89–94.

27 P. A. Troshin, D. K. Susarova, E. A. Khakina, A. A. Goryachev, O. V. Borshchev, S. A. Ponomarenko, V. F. Razumov and N. S. Sariciftci, *J. Mater. Chem.*, 2012, **22**, 18433.

28 G. E. Morse, A. lien Tournebize, B. Agnè Rivaton, T. Chassé, C. Taviot-Gueho, N. Blouin, O. R. Lozman and S. Tierney, *Phys. Chem. Chem. Phys.*, 2015, **17**, 11884–11897.

29 A. Distler, T. Sauermann, H. J. Egelhaaf, S. Rodman, D. Waller, K. S. Cheon, M. Lee and D. M. Guldi, *Adv. Energy Mater.*, 2014, **4,** 1300693.

30 G. D. Spyropoulos, C. O. Ramirez Quiroz, M. Salvador, Y. Hou, N. Gasparini, P. Schweizer, J. Adams, P. Kubis, N. Li, E. Spiecker, T. Ameri, H. Egelhaaf and C. J. Brabec, *Energy Environ. Sci.*, 2016, **9**, 2302–2313.

31 F. MacHui, S. Langner, X. Zhu, S. Abbott and C. J. Brabec, *Sol. Energy Mater. Sol. Cells*, 2012, **100**, 138–146.

32 S. Berny, N. Blouin, A. Distler, H. Egelhaaf, M. Krompiec, A. Lohr, O. R. Lozman, G. E. Morse, L. Nanson, A. Pron, T. Sauermann, N. Seidler, S. Tierney, P. Tiwana, M. Wagner and H. Wilson, *Adv. Sci.*, 2016, **3**, 1500342.

33 M. Bolognesi, M. Prosa, M. Tessarolo, G. Donati, S. Toffanin, M. Muccini and M. Seri, *Sol. Energy Mater. Sol. Cells*, 2016, **155**, 436–445.

34 V. Vohra, K. Kawashima, T. Kakara, T. Koganezawa, I. Osaka, K. Takimiya and H. Murata, *Nat. Photonics*, 2015, **9**, 403–408.

35 Y. Santo, I. Jeon, K. Sheng Yeo, T. Nakagawa and Y. Matsuo, *Appl. Phys. Lett.*, 2013, **103**, 73306.

36 K. A. Mazzio and C. K. Luscombe, *Chem. Soc. Rev.*, 2015, **44**, 78–90.

37 R. Po, G. Bianchi, C. Carbonera and A. Pellegrino, *Macromolecules*, 2015, **48**, 453–461.

38 W. Si, X. Zhang, S. Lu, T. Yasuda, N. Asao, L. Han, Y. Yamamoto and T. Jin, *Sci. Rep.*, 2015, **5**, 13920.

39 H. Tanaka, Y. Abe, Y. Matsuo, J. Kawai, I. Soga, Y. Sato and E. Nakamura, *Adv. Mater.*, 2012, **24**, 3521–3525.

40 V. D. Mihailetchi, H. X. Xie, B. deBoer, L. J. A. Koster and P. W. M. Blom, *Adv. Funct. Mater.*, 2006, **16**, 699–708.

41 V. D. Mihailetchi, J. K. J. van Duren, P. W. M. Blom, J. C. Hummelen, R. A. J. Janssen, J. M. Kroon, M. T. Rispens, W. J. H. Verhees and M. M. Wienk, *Adv. Funct. Mater.*, 2003, **13**, 43–46.

42 K. Kawashima, Y. Tamai, H. Ohkita, I. Osaka and K. Takimiya, *Nat. Commun.*, 2015, **6**, 10085.

43 I. Jeon and Y. Matsuo, *Sol. Energy Mater. Sol. Cells*, 2015, **140**, 335–343.

44 Z. Xu, L. M. Chen, G. Yang, C. H. Huang, J. Hou, Y. Wu, G. Li, C. S. Hsu and Y. Yang, *Adv. Funct. Mater.*, 2009, **19**, 1227–1234.

45 J. Kettle, Z. Ding, M. Horie and G. C. Smith, *Org. Electron.,* 2016, **39**, 222–228.

46 M.-G. Jeong, H. O. Seo, D. H. Kim, K.-D. Kim, E. J. Park, Y. D. Kim and D. C. Lim, *J. Phys. Chem. C*, 2014, **118**, 3483–3489.

47 H. O. Seo, M.-G. Jeong, K.-D. Kim, D. H. Kim, Y. D. Kim and D. C. Lim, *Surf. Interface Anal.* 2014, **46**, 544–549.

48 D. H. Kim, M.-G. Jeong, H. O. Seo and Y. D. Kim, *Phys. Chem. Chem. Phys.,* 2015, **17**, 599–604.

49 J. Jeong, J. Seo, S. Nam, H. Han, H. Kim, T. D. Anthopoulos, D. D. C. Bradley and Y. Kim *Adv. Sci.,* 2016, **3,** 1500269.

50 W. R. Wu, U. S. Jeng, C. J. Su, K. H. Wei, M. S. Su, M. Y. Chiu, C. Y. Chen, W. Bin Su, C. H. Su and A. C. Su, *ACS Nano*, 2011, **5**, 6233–6243.